



Anomalous Cyclotron Motion in Graphene Superlattice Cavities

Rainer Kraft,^{1,2,*} Ming-Hao Liu (劉明豪) ,^{3,†} Pranaav Balaji Selvasundaram,^{1,4} Szu-Chao Chen (陳思超),³
 Ralph Krupke,^{1,4,5} Klaus Richter,⁶ and Romain Danneau ^{1,5,‡}

¹*Institute of Nanotechnology, Karlsruhe Institute of Technology, Karlsruhe D-76021, Germany*

²*Institute of Physics, Karlsruhe Institute of Technology, Karlsruhe D-76049, Germany*

³*Department of Physics, National Cheng Kung University, Tainan 70101, Taiwan*

⁴*Department of Materials and Earth Sciences, Technical University Darmstadt, Darmstadt D-64287, Germany*

⁵*Institute for Quantum Materials and Technologies, Karlsruhe Institute of Technology, Karlsruhe D-76021, Germany*

⁶*Institut für Theoretische Physik, Universität Regensburg, Regensburg D-93040, Germany*



(Received 8 April 2020; accepted 20 October 2020; published 17 November 2020)

We consider graphene superlattice miniband fermions probed by electronic interferometry in magneto-transport experiments. By decoding the observed Fabry-Pérot interference patterns together with our corresponding quantum transport simulations, we find that the Dirac quasiparticles originating from the superlattice minibands do not undergo conventional cyclotron motion but follow more subtle trajectories. In particular, dynamics at low magnetic fields is characterized by peculiar, straight trajectory segments. Our results provide new insights into superlattice miniband fermions and open up novel possibilities to use periodic potentials in electron optics experiments.

DOI: [10.1103/PhysRevLett.125.217701](https://doi.org/10.1103/PhysRevLett.125.217701)

The presence of a superlattice potential modulates the intrinsic electronic band structure of a material [1], allowing the observation of various physical phenomena such as Wannier-Stark ladders [2] or Weiss and Bloch oscillations [3,4]. In graphene, superimposed long-range periodic potentials are predicted to alter the electronic dispersion with the emergence of extra singularities and new effective Dirac fermions [5–7]. Thanks to the rapid development of artificial two-dimensional van der Waals (vdW) heterostructures, studying superlattice effects in graphene is nowadays possible [8–11]. For instance, when a graphene sheet is placed onto a hexagonal boron nitride (hBN) crystallite, interference due to the small lattice constant mismatch of about 1.8% gives rise to a moiré pattern with a superstructure lattice parameter inversely proportional to the rotational misalignment between the layers. Strikingly, while secondary Dirac points appear in the modulated electronic band structure [12], magnetotransport measurements revealed the Hofstadter butterfly [13–15] as well as magnetic Bloch states via the observation of Brown-Zak oscillations [13,16,17]. The latter highlights a particular metallic behavior with straight trajectories of the quasiparticles at relatively high magnetic field, i.e., at values of the magnetic flux per superlattice unit cell area commensurate with the magnetic flux quantum. At low magnetic field the impact of the superlattice on the quasiparticles has been studied by transverse electron focusing experiments showing that cyclotron motions break down near the secondary Dirac points [18]. However, studying and distinguishing the transport behaviors of charge carriers due to superlattice minibands from

those arising from the normal Dirac spectrum in the absence of magnetic field, as well as the crossover to the intermediate field regime, remains very challenging.

Here, we report a study of superlattice Dirac fermion transport in a hBN/graphene/hBN heterostructure through an electrostatically defined cavity formed by a local top gate (TG) and an overall back gate (BG) [see Fig. 1(a) and Supplemental Material Sec. I for more details [19]]. The combination of the two gates allows independent control over the charge carrier densities n_{in} and n_{out} in inner and outer regions of the device, respectively. Because of semitransparent boundaries in a bipolar configuration (i.e., transitions across the charge neutrality point between inner and outer regions) a Fabry-Pérot (FP) cavity forms, where the interference of partially reflected and transmitted ballistic charge carrier trajectories gives rise to conductance oscillations [32–35]. In the case of a moiré superlattice the transitions across secondary Dirac points result in the formation of extra cavities [36] (see Supplemental Material, Secs. II–IV for more details on the basic properties of the device and the cavities [19]). By investigating the unusual cavity properties and probing the arising interferences via magnetotransport measurements, as well as quantum transport simulations, we are able to study the moiré miniband conduction associated with unconventional Dirac quasiparticle dynamics. Figures 1(b), 1(c) display a schematic of the simulated device geometry with superimposed periodic long-range potential as the scattering region [37,38], and the corresponding electronic band structure obtained from the continuum model, respectively (details given in Ref. [38]).

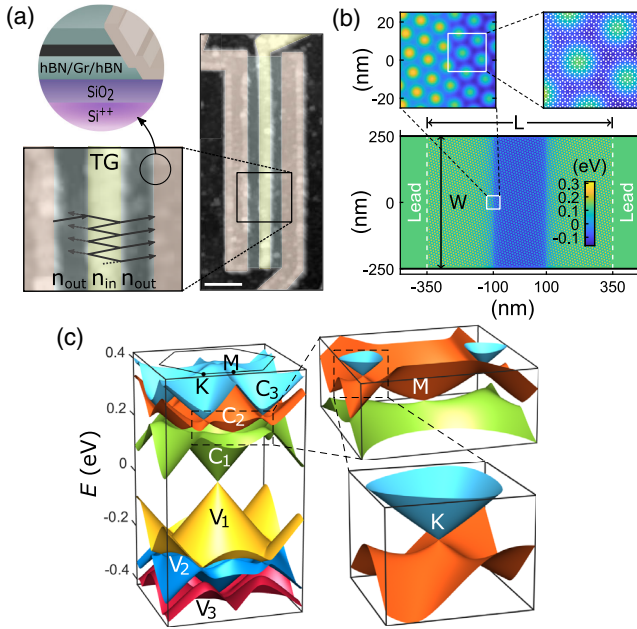


FIG. 1. (a) False-color AFM image of the device (scale bar $1 \mu\text{m}$). The local top gate (TG, yellow) in the center forms in combination with the overall back gate (BG, green) a Fabry-Pérot cavity. Partially reflected and transmitted ballistic trajectories in this electronic interferometer are indicated by small arrows. The magnified region of the contact interface depicts a schematic of the edge-connected hBN/graphene/hBN vdW heterostructure. (b) Schematic of the modeled device, showing the (scaled) graphene lattice as the scattering region with a superimposed periodic long-range potential. (c) Corresponding electronic band structure of a single-layer graphene with electrostatic superlattice based on the continuum model. Close-ups of the minibands at special points M and K of the superlattice mini-Brillouin zone are shown on the right.

The effect of the superlattice in graphene is directly observed in transport experiments and a moiré wavelength $\lambda \approx 10.9 \text{ nm}$ is extracted from the analysis of the Brown-Zak oscillations (see Supplemental Material, Secs. IV and V for more details [19]). As overview on the density-dependent device characteristics, Figs. 2(a), 2(b) show maps of the conductance as a function of n_{in} and n_{out} obtained from experimental measurement and quantum transport simulation, respectively. The conductance profile is structured by the appearance of the main Dirac point at vanishing densities [highlighted by black dashed lines in Fig. 2(b)] and satellite Dirac points on electron-side and hole-side [highlighted by cyan and magenta dashed lines in Fig. 2(b)], resulting in a map composed of 16 regions of unique doping configurations. To facilitate the following discussions, we introduce a notation with small letters p and n describing charge carriers within the linear valence band V_1 and conduction band C_1 of the original primary Dirac cone, while capital letters P and N denote charge carriers in the backfolded superlattice minibands (V_2, V_3 , and C_2, C_3) below and above the secondary Dirac points,

respectively. The labeling of each junction configuration is shown in Fig. 2(b). We note that in the experimental map the two regions on the upper left corner (NPN) and lower right corner (PNP) are missing, corresponding to the most extreme opposite doping between inner and outer regions where applied TG and BG voltages counteract in the dual-gated part of the device.

In both maps we observe multiple sets of FP interferences originating from the different cavity combinations. Notably, in addition to the well-known resonances in the bipolar regions npn and pnp [32–35], interference patterns are visible in the nominal unipolar quadrants of an ordinary graphene p - n junction device. Here, cavities can be formed where the interfaces between regions of charge carriers from the normal Dirac spectrum and superlattice minibands play the role of semitransparent boundaries rather than p - n interfaces (cf. Ref. [36]). Indeed, the coexistence of both junction types can be strikingly observed in Fig. 2(a) with two superimposed but distinct sets of FP interferences in $n\text{Pn}$ (pNp). For these configurations, the spatial density profile from inner to outer regions features transitions first across the satellite Dirac point and then across the primary Dirac point [see Fig. 2(c)]. Hence, the inner most cavity is formed in the same fashion as in pPp (nNn) and, consequently, oscillation fringes originating in pPp (nNn) remain visible across the main Dirac peak of the outer charge carrier density axis. We note that in the simulated map [Fig. 2(b)] the continuation of the fringes is only faintly visible in pNp .

We now compare the behavior of a “common” p - n - p junction with a cavity formed by the satellite Dirac points, focusing on configurations npn , pnp , and pPp , nNn [see Fig. 2(c) for corresponding spatial density profiles]. Though it should be mentioned that the moiré superlattice potential is always present in both inner and outer regions, only the Fermi level is spatially tuned by the BG and TG to reside within the different bands of the reconstructed band structure (unlike the transition from a nonsuperlattice to superlattice region as, e.g., proposed in Ref. [39]). It is already visible from the maps [Figs. 2(a), 2(b)] that the spacing of the resonances in pPp and nNn appears notably increased in comparison to cavities npn and pnp . In Fig. 2(d) the extracted density spacing is plotted as a function of n_{in} for exemplary linecuts at constant n_{out} . The enlarged oscillation period can be attributed to a suddenly reduced cavity size due to the newly defined boundaries by the satellite Dirac points. Figure 2(e) shows the observed drop in the experimentally extracted cavity size $L = \pi/\Delta k_F$, where $\Delta k_F = |k_{F,j+1} - k_{F,j}|$ with $k_F = \sqrt{\pi n}$ and j the interference maximum index, following in good agreement the trend of a numerical determination of the cavity size from electrostatic simulations (black dashed lines).

To further explore the charge carrier behavior in the superlattice minibands, we have studied the four different cavities with applied B (as well as by source-drain bias

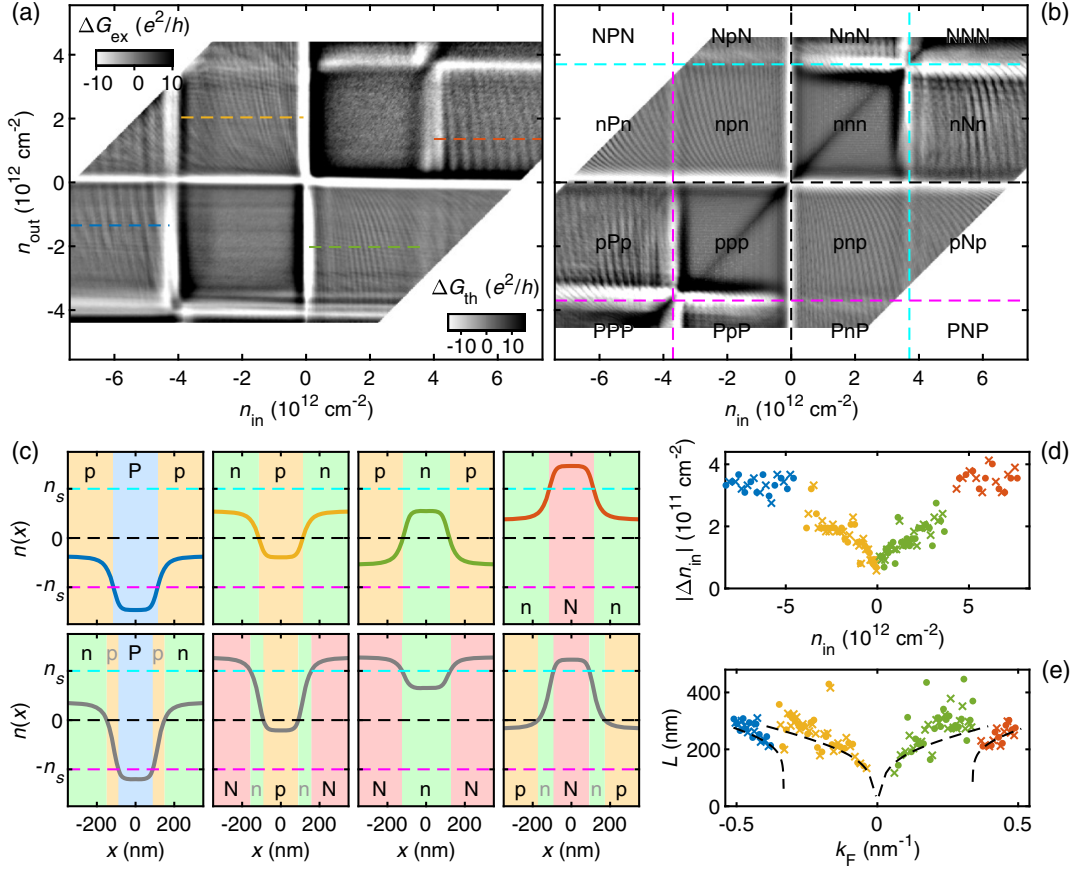


FIG. 2. (a), (b) Measured and simulated map of the conductance with subtracted smooth background, respectively, as a function of n_{in} and n_{out} . Labels denote the charge carrier configurations in all 16 quadrants, which are defined by the main Dirac point (black dashed lines) and hole or electron satellite Dirac point (magenta or cyan dashed lines). (c) Spatial density profiles across the device for different doping scenarios. (d) Density spacing between resonances as a function of n_{in} for the cavities pPp (blue), npn (orange), pnp (green), and nNn (red) at constant outer charge carrier densities $n_{out} = -1.4 \times 10^{12}$, 2.0×10^{12} , -2.0×10^{12} , and $1.4 \times 10^{12} \text{ cm}^{-2}$, respectively, as marked by the colored dashed lines in panel (a). (e) Corresponding cavity size L as a function of Fermi wave vector k_F . The black dashed lines show a numerical determination of the cavity size obtained from electrostatic simulations.

spectroscopy, shown in the Supplemental Material, Sec. VI [19]. Figures 3(a), 3(b) show maps of the measured and simulated FP interference patterns as a function of n_{in} and magnetic field B at constant n_{out} (see Supplemental Material Sec. VII for additional patterns at different n_{out} [19]). The resulting patterns in npn and pnp of both simulation and experiment show fringes with typical dispersing behavior towards higher densities with increasing B due to the competition of the Aharonov-Bohm phase and Wentzel-Kramer-Brillouin kinetic phase, as well as the appearance of a π shift as the hallmark of Klein tunneling in monolayer graphene [32,40–42]. However, strikingly different patterns are observed in the case of pPp and nNn. Here, no π shift is visible and fringes do not or only weakly disperse under the influence of B , which implies a lacking of a magnetic-field-dependent phase. Moreover, the resonances in nNn vanish abruptly at $B_c \sim 300$ mT, while in pPp the oscillation fringes remain visible, yet less pronounced. Nevertheless, the nondispersing fringes are monitored in both cases.

In order to understand why the miniband charge carriers do not pick up a magnetic phase, we have investigated their trajectories by performing quantum transport simulations using a narrow beam injector into a wider 2D sample (see Supplemental Material Sec. VIII for details [19]). The left panel of Fig. 3(c) depicts the energy band dispersions along symmetry points, where the red shaded region marks the energy window corresponding to nondispersing fringes in nNn of Fig. 3(b). The resulting trajectory beams for two distinct Fermi levels [red and green horizontal dashed lines on the band diagram of Fig. 3(c)] are shown on the right-hand side at various B . In the case of normal Dirac fermions originating from the primary Dirac cone [C_1 band of Fig. 1(c)], the simulated beams [lower row of Fig. 3(c)] follow the expected cyclotron motion of moving charge carriers in a magnetic field (the purple dashed lines correspond to the calculated cyclotron radius $r_c = \hbar k_F / eB$). In the other case [upper row of Fig. 3(c)], where miniband Dirac fermions originate from C_2 and C_3 bands, the simulated beams persist on a quasistraight

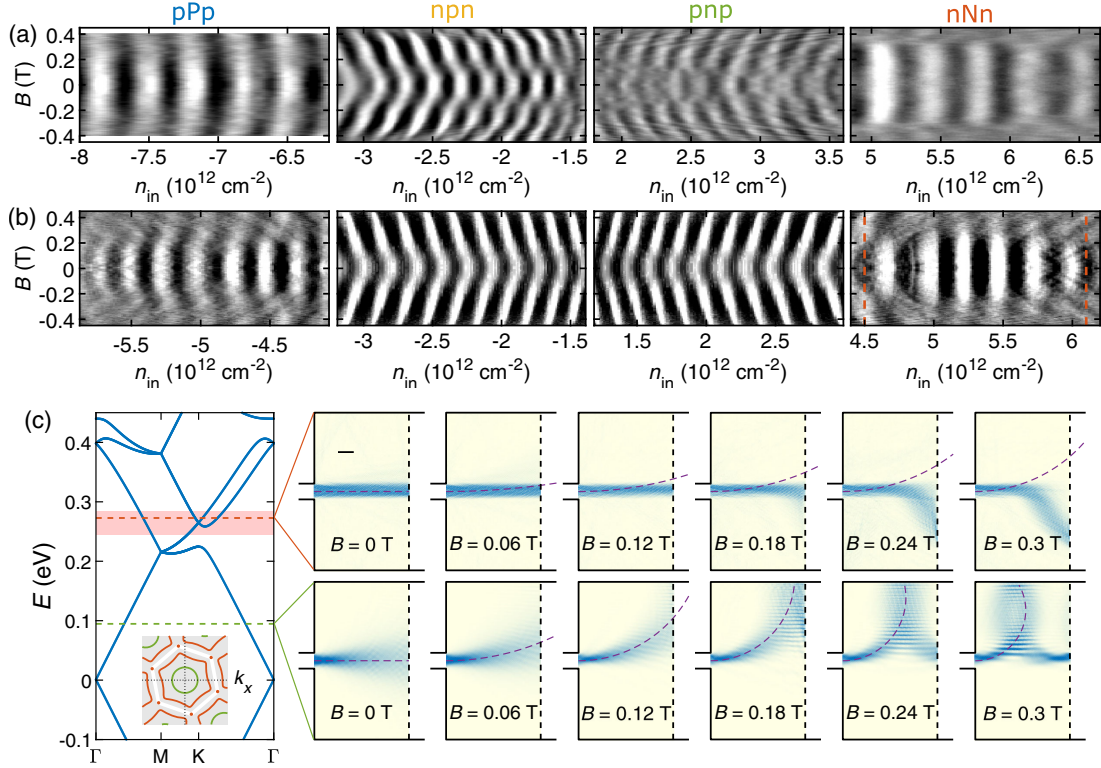


FIG. 3. Low magnetic field measurements of the four different cavities pPp, npn, pnp, and nNn in column-wise order at constant outer charge carrier densities $n_{\text{out}} = -1.4 \times 10^{12}$, 2.0×10^{12} , -2.0×10^{12} , and $1.4 \times 10^{12} \text{ cm}^{-2}$, respectively. (a), (b) Experimental and simulated patterns of the conductance oscillations, respectively, as a function of charge carrier density n_{in} and B . (c) Band structure of our superlattice model, with the red shaded region denoting the energy window of nondispersing fringes in nNn. The inset depicts the Fermi surface slightly above the K point of the mini-Brillouin zone marked by the red dashed line. Right-hand side panels: charge carrier beams are shown from simulations for varying B at two different Fermi levels at distinctly different band structure regions. Upper row: C_2 and C_3 minibands (red dashed line) Lower row: C_1 band of the primary Dirac cone (green dashed line).

trajectory on the length scale of the cavity for small B , which explains the absence of the magnetic field dependent phase in the FP interference patterns.

The observed unusual B independence of the beam can be understood as the consequence of a reshaped Fermi surface of the superlattice minibands, shown as inset in the left panel of Fig. 3(c) for the two scenarios discussed above (green and red indicated Fermi levels, respectively). Following from the semiclassical equation of motion $\hbar \dot{\mathbf{k}} = q(\mathbf{E} + \dot{\mathbf{r}} \times \mathbf{B})$ (for a full description, see Chap. 12 of Ref. [43]) the cyclotron orbit in real space is given by the orbit in momentum space rotated by 90° . Indeed, in the red scenario (miniband Dirac fermions) of Fig. 3(c) with increasing B , the hexagonal bending of the trajectories in the opposite rotation direction compared to the green scenario (normal Dirac fermions), directly reflects the hole-type hexagonal Fermi contour of C_2 . In fact, the half length of the side of the hexagonlike trajectory is found to reduce to the size of the top-gate-defined cavity at around $B \sim 0.3 \text{ T}$, within which the incident angle of the miniband Dirac fermion remains nearly perpendicular to the cavity interface, leading to B independent FP interference fringes. At $B \gtrsim 0.3 \text{ T}$, the incident angle significantly increases,

leading to the disappearance of the FP interference (see Supplemental Material, Fig. S12 [19]).

Finally, we observed different B dependence of FP interferences in NpN and NnN, where normal Dirac fermions are confined to the cavity. Yet, the same argument of the reshaped Fermi surface holds to explain the distinct behaviors. In the case of NnN, the almost normal incident angle of superlattice quasiparticles from the outer reservoirs onto the cavity interfaces prevents the confined electrons to form closed loops inside the cavity. At a given B , where the hexagonal orbital bending of the outside miniband fermions occurs on a length scale shorter than the outer reservoirs, the resonances vanish similar to the reversed configuration nNn. On the other hand, NpN features transitions across both primary and secondary Dirac points [see Fig. 2(c)]. Since the innermost cavity resembles npn, a continuation of interference fringes from npn to NpN in the maps of Figs. 2(a), 2(b) can be observed, and the magnetic field behavior of the conductance resonances conforms with ordinary n-p-n junctions.

To conclude, we have probed the transport properties of charge carriers in a graphene/hBN moiré superlattice device by electronic interferometry. The nondispersing fringes of

FP interferences at low magnetic field combined with our quantum transport simulations revealed unconventional cyclotron motion on the length scale of the cavity, which reflect the reshaped hexagonal Fermi surface. The subtle transport properties of these quasiparticles provide a new versatile platform for new types of devices in electron optics experiments, which could be used to probe, for example, correlated states in twisted bilayers [44–48].

The authors thank Í. Adagideli, I. Gornyi, A. Knothe, P. Makk, C. Schönenberger, and O. Zilberberg for fruitful discussions. This work was supported by the Helmholtz society through the STN program, the German Research foundation (DFG, Deutsche Forschungsgemeinschaft) Project-ID 314695032-CRC1277 and through the Project Ri681/13-1, as well as the Taiwan Ministry of Science (107-2112-M-006-004-MY3, 107-2627-E-006-001, and 109-2112-M-006-020-MY3) and Ministry of Education (Higher Education Sprout Project).

*rainer.kraft@kit.edu

†minghao.liu@phys.ncku.edu.tw

‡romain.danneau@kit.edu

- [1] L. Esaki and R. Tsu, Superlattice and negative conductivity in semiconductors, *IBM J. Res. Dev.* **14**, 61 (1970).
- [2] E. E. Mendez, F. Agullo-Rueda, and J. M. Hong, Stark Localization in GaAs-GaAlAs Superlattices under an Electric Field, *Phys. Rev. Lett.* **60**, 2426 (1988).
- [3] D. Weiss, K. von Klitzing, K. Ploog, and G. Weimann, Magnetoresistance oscillations in a two-dimensional electron gas induced by a submicrometer periodic potential, *Europhys. Lett.* **8**, 179 (1989).
- [4] C. Waschke, H. G. Roskos, R. Schwedler, K. Leo, H. Kurz, and K. Köhler, Coherent Submillimeter-wave Emission from Bloch Oscillations in a Semiconductor Superlattice, *Phys. Rev. Lett.* **70**, 3319 (1993).
- [5] C.-H. Park, L. Yang, Y.-W. Son, M. L. Cohen, and S. G. Louie, New Generation of Massless Dirac Fermions in Graphene under External Periodic Potentials, *Phys. Rev. Lett.* **101**, 126804 (2008).
- [6] C.-H. Park, L. Yang, Y.-W. Son, M. L. Cohen, and S. G. Louie, Anisotropic behaviours of massless Dirac fermions in graphene under periodic potentials, *Nat. Phys.* **4**, 213 (2008).
- [7] M. Barbier, P. Vasilopoulos, and F. M. Peeters, Extra Dirac points in the energy spectrum for superlattices on single-layer graphene, *Phys. Rev. B* **81**, 075438 (2010).
- [8] M. Yankowitz, Q. Ma, P. Jarillo-Herrero, and B. J. LeRoy, van der Waals heterostructures combining graphene and hexagonal boron nitride, *Nat. Rev. Phys.* **1**, 112 (2019).
- [9] C. Forsythe, X. Zhou, K. Watanabe, T. Taniguchi, A. Pasupathy, P. Moon, M. Koshino, P. Kim, and C. R. Dean, Band structure engineering of 2D materials using patterned dielectric superlattices, *Nat. Nanotechnol.* **13**, 566 (2018).
- [10] M. Drienovsky, J. Joachimsmeier, A. Sandner, M.-H. Liu, T. Taniguchi, K. Watanabe, K. Richter, D. Weiss, and J. Eroms, Commensurability Oscillations in One-Dimensional Graphene Superlattices, *Phys. Rev. Lett.* **121**, 026806 (2018).
- [11] R. Huber, M.-H. Liu, S.-C. Chen, M. Drienovsky, A. Sandner, K. Watanabe, T. Taniguchi, K. Richter, D. Weiss, and J. Eroms, Tunable two-dimensional superlattices in graphene, *Nano. Lett.* **20**, 8046 (2020).
- [12] M. Yankowitz, J. Xue, D. Cormode, J. D. Sanchez-Yamagishi, K. Watanabe, T. Taniguchi, P. Jarillo-Herrero, P. Jacquod, and B. J. LeRoy, Emergence of superlattice Dirac points in graphene on hexagonal boron nitride, *Nat. Phys.* **8**, 382 (2012).
- [13] L. A. Ponomarenko, R. V. Gorbachev, G. L. Yu, D. C. Elias, R. Jalil, A. A. Patel, A. Mishchenko, A. S. Mayorov, C. R. Woods, J. R. Wallbank, M. Mucha-Kruczynski, B. A. Piot, M. Potemski, I. V. Grigorieva, K. S. Novoselov, F. Guinea, V. I. Fal'ko, and A. K. Geim, Cloning of Dirac fermions in graphene superlattices, *Nature (London)* **497**, 594 (2013).
- [14] C. R. Dean, L. Wang, P. Maher, C. Forsythe, F. Ghahari, Y. Gao, J. Katoch, M. Ishigami, P. Moon, M. Koshino, T. Taniguchi, K. Watanabe, K. L. Shepard, J. Hone, and P. Kim, Hofstadter's butterfly and the fractal quantum Hall effect in Moiré superlattices, *Nature (London)* **497**, 598 (2013).
- [15] B. Hunt, J. D. Sanchez-Yamagishi, A. F. Young, M. Yankowitz, B. J. LeRoy, K. Watanabe, T. Taniguchi, P. Moon, M. Koshino, P. Jarillo-Herrero, and R. C. Ashoori, Massive Dirac fermions and hofstadter butterfly in a van der Waals heterostructure, *Science* **340**, 1427 (2013).
- [16] R. K. Kumar, X. Chen, G. H. Auton, A. Mishchenko, D. A. Bandurin, S. V. Morozov, Y. Cao, E. Khestanova, M. B. Shalom, A. V. Kretinin, K. S. Novoselov, L. Eaves, I. V. Grigorieva, L. A. Ponomarenko, V. I. Fal'ko, and A. K. Geim, High-temperature quantum oscillations caused by recurring Bloch states in graphene superlattices, *Science* **357**, 181 (2017).
- [17] G. Chen, M. Sui, D. Wang, S. Wang, J. Jung, P. Moon, S. Adam, K. Watanabe, T. Taniguchi, S. Zhou, M. Koshino, G. Zhang, and Y. Zhang, Emergence of tertiary Dirac points in graphene Moiré superlattices, *Nano Lett.* **17**, 3576 (2017).
- [18] M. Lee, J. R. Wallbank, P. Gallagher, K. Watanabe, T. Taniguchi, V. I. Fal'ko, and D. Goldhaber-Gordon, Ballistic miniband conduction in a graphene superlattice, *Science* **353**, 1526 (2016).
- [19] See Supplemental Material at <http://link.aps.org/supplemental/10.1103/PhysRevLett.125.217701> for experimental details, description of our quantum transport simulations, the uniform doping characteristics, the analysis of the Brown-Zak oscillations, the source-drain bias spectroscopy study of several cavities, as well as additional data on the Fabry-Perot cavity characteristics and figures, which includes Refs. [20–31].
- [20] L. Wang, I. Meric, P. Y. Huang, Q. Gao, Y. Gao, H. Tran, T. Taniguchi, K. Watanabe, L. M. Campos, D. A. Muller, J. Guo, P. Kim, J. Hone, K. L. Shepard, and C. R. Dean, One-dimensional electrical contact to a two-dimensional material, *Science* **342**, 614 (2013).
- [21] R. Kraft, J. Mohrmann, R. Du, P. B. Selvasundaram, M. Irfan, U. N. Kanilmaz, F. Wu, D. Beckmann, H. von Löhneysen, R. Krupke, A. Akhmerov, I. Gornyi, and R.

- Danneau, Tailoring supercurrent confinement in graphene bilayer weak links, *Nat. Commun.* **9**, 1722 (2018).
- [22] X. Du, I. Skachko, A. Barker, and E. Y. Andrei, Approaching ballistic transport in suspended graphene, *Nat. Nanotechnol.* **3**, 491 (2008).
- [23] S. Cho and M. Fuhrer, Massless and massive particle-in-a-box states in single- and bi-layer graphene, *Nano Res.* **4**, 385 (2011).
- [24] F. Wu, P. Queipo, A. Nasibulin, T. Tsuneta, T. H. Wang, E. Kauppinen, and P. J. Hakonen, Shot Noise with Interaction Effects in Single-walled Carbon Nanotubes, *Phys. Rev. Lett.* **99**, 156803 (2007).
- [25] P. Pandey, R. Kraft, R. Krupke, D. Beckmann, and R. Danneau, Andreev reflection in ballistic normal metal/graphene/superconductor junctions, *Phys. Rev. B* **100**, 165416 (2019).
- [26] D. I. Indolese, R. Delagrangé, P. Makk, J. R. Wallbank, K. Watanabe, T. Taniguchi, and C. Schönberger, Signatures of van Hove Singularities Probed by the Supercurrent in a Graphene-hBN Superlattice, *Phys. Rev. Lett.* **121**, 137701 (2018).
- [27] A. Cresti, R. Farchioni, G. Grosso, and G. P. Parravicini, Keldysh-Green function formalism for current profiles in mesoscopic systems, *Phys. Rev. B* **68**, 075306 (2003).
- [28] B. K. Nikolić, L. P. Zarbo, and S. Souma, Imaging mesoscopic spin Hall flow: Spatial distribution of local spin currents and spin densities in and out of multiterminal spin-orbit coupled semiconductor nanostructures, *Phys. Rev. B* **73**, 075303 (2006).
- [29] M.-H. Liu, C. Gorini, and K. Richter, Creating and Steering Highly Directional Electron Beams in Graphene, *Phys. Rev. Lett.* **118**, 066801 (2017).
- [30] P. Moon and M. Koshino, Electronic properties of graphene/hexagonal-boron-nitride Moiré superlattice, *Phys. Rev. B* **90**, 155406 (2014).
- [31] J. R. Wallbank, M. Mucha-Kruczyński, and V. I. Fal'ko, Moiré superlattice effects in graphene/boron-nitride van der Waals heterostructures, *Ann. Phys. (Amsterdam)* **527**, 359 (2015).
- [32] A. F. Young and P. Kim, Quantum interference and Klein tunnelling in graphene heterojunctions, *Nat. Phys.* **5**, 222 (2009).
- [33] L. C. Campos, A. F. Young, K. Surakitbovorn, K. Watanabe, T. Taniguchi, and P. Jarillo-Herrero, Quantum and classical confinement of resonant states in a Trilayer graphene Fabry-Pérot interferometer, *Nat. Commun.* **3**, 1239 (2012).
- [34] A. Varlet, M.-H. Liu, V. Krueckl, D. Bischoff, P. Simonet, K. Watanabe, T. Taniguchi, K. Richter, K. Ensslin, and T. Ihn, Fabry-Pérot Interference in Gapped Bilayer Graphene with Broken Anti-Klein Tunneling, *Phys. Rev. Lett.* **113**, 116601 (2014).
- [35] R. Du, M.-H. Liu, J. Mohrmann, F. Wu, R. Krupke, H. von Löhneysen, K. Richter, and R. Danneau, Tuning Anti-Klein to Klein Tunneling in Bilayer Graphene, *Phys. Rev. Lett.* **121**, 127706 (2018).
- [36] C. Handschin, P. Makk, P. Rickhaus, M.-H. Liu, K. Watanabe, T. Taniguchi, K. Richter, and C. Schönberger, Fabry-Pérot resonances in a graphene/hBN Moiré superlattice, *Nano Lett.* **17**, 328 (2017).
- [37] M.-H. Liu, P. Rickhaus, P. Makk, E. Tóvári, R. Maurand, F. Tkatschenko, M. Weiss, C. Schönberger, and K. Richter, Scalable Tight-Binding Model for Graphene, *Phys. Rev. Lett.* **114**, 036601 (2015).
- [38] S.-C. Chen, R. Kraft, R. Danneau, K. Richter, and M.-H. Liu, Electrostatic superlattices on scaled graphene lattices, *Commun. Phys.* **3**, 71 (2020).
- [39] C. W. J. Beenakker, N. V. Gnezdilov, E. Dresselhaus, V. P. Ostroukh, Y. Herasymenko, Í. Adagideli, and J. Tworzydło, Valley switch in a graphene superlattice due to Pseudo-Andreev reflection, *Phys. Rev. B* **97**, 241403(R) (2018).
- [40] M. I. Katsnelson, *Graphene: Carbon in Two Dimensions* (Cambridge University Press, Cambridge, England, 2012).
- [41] A. V. Shytov, M. S. Rudner, and L. S. Levitov, Klein Backscattering and Fabry-Pérot Interference in Graphene Heterojunctions, *Phys. Rev. Lett.* **101**, 156804 (2008).
- [42] P. Rickhaus, P. Makk, M.-H. Liu, E. Tóvári, M. Weiss, R. Maurand, K. Richter, and C. Schönberger, Snake trajectories in ultraclean graphene p-n junctions, *Nat. Commun.* **6**, 6470 (2015).
- [43] N. W. Ashcroft and N. D. Mermin, *Solid State Physics* (Holt, Rinehart and Winston, New York, 1977).
- [44] Y. Cao, V. Fatemi, S. Fang, K. Watanabe, T. Taniguchi, E. Kaxiras, and P. Jarillo-Herrero, Unconventional superconductivity in magic-angle graphene superlattices, *Nature (London)* **556**, 43 (2018).
- [45] Y. Cao, V. Fatemi, A. Demir, S. Fang, S. L. Tomarken, J. Y. Luo, J. D. Sanchez-Yamagishi, K. Watanabe, T. Taniguchi, E. Kaxiras, R. C. Ashoori, and P. Jarillo-Herrero, Correlated insulator behaviour at half-filling in magic-angle graphene superlattices, *Nature (London)* **556**, 80 (2018).
- [46] A. L. Sharpe, E. J. Fox, A. W. Barnard, J. Finney, K. Watanabe, T. Taniguchi, M. A. Kastner, and D. Goldhaber-Gordon, Emergent ferromagnetism near three-quarters fillings in twisted bilayer graphene, *Science* **365**, 605 (2019).
- [47] X. Lu, P. Stepanov, W. Yang, M. Xie, M. A. Aamir, I. Das, C. Urgell, K. Watanabe, T. Taniguchi, G. Zhang, A. Bachtold, A. H. MacDonald, and D. K. Efetov, Superconductors, orbital magnets and correlated states in magic-angle bilayer graphene, *Nature (London)* **574**, 653 (2019).
- [48] C. Shen, Y. Chu, Q. Wu, N. Li, S. Wang, Y. Zhao, J. Tang, J. Liu, J. Tian, K. Watanabe, T. Taniguchi, R. Yang, Z. Y. Meng, D. Shi, O. V. Yazyev, and G. Zhang, Correlated states in twisted double bilayer graphene, *Nat. Phys.* **16**, 520 (2020).